Talanta Open 9 (2024) 100279

Contents lists available at ScienceDirect

Talanta Open

journal homepage: www.sciencedirect.com/journal/talanta-open

Digital-movie-based flow colorimetry for pH measurement with universal indicators

Selass Kebede Olbemo [a], Masaki Takeuchi [a,b], Hideji Tanaka [a,b,*]

[a] Graduate School of Pharmaceutical Sciences, Tokushima University, 1-78-1 Shomachi, Tokushima 770-8505, Japan
[b] Institute of Biomedical Sciences, Tokushima University, 1-78-1 Shomachi, Tokushima 770-8505, Japan

ARTICLE INFO

Keywords:
pH
Digital movie-based colorimetry
Universal indicator
RGB
Hue

ABSTRACT

A continuous, simple, and versatile pH monitoring method based on digital-movie-based colorimetry is proposed. A constructed flow system was of a two-channel configuration mainly composed of two peristaltic pumps, a digital microscope-based detector, a pH meter with a flow-through combination pH-reference electrode, and a laptop computer. While the total flow rate (F_T) was held constant, the flow rate (F_B) of a base solution for Britton-Robinson buffer containing a universal indicator (Yamada's indicator or Van Urik's indicator) was changed in proportion to the control signal (V_c) from the computer. An acid solution for the buffer containing the indicator was aspirated to the confluence point at the flow rate of $F_T - F_B$ and mixed with the base solution. Thus, buffer solutions with arbitrary pH could be easily prepared. The image of the mixed solution was captured with the microscope downstream; the pH of the solution was measured with the pH meter at the most downstream. An in-house program written in Visual Basic .NET was developed to control the system, acquire and analyze the signals (image data and pH), and display the results automatically; the color of the image was expressed as tristimulus values (i.e., *R, G, B*), hue, and luminance. The relationships between these color-specific values and pH were analyzed after optimizing the V_c scan rate. Van Uik's indicator was superior to Yamada's regarding the applicable pH range (ca. 2.5 – 10). A sigmoid-like calibration curve was established between hue and pH, which was used to determine sample pH. The proposed method was validated by measuring the pH of different drugs and vinegar samples.

Introduction

pH is a measure of the acidity or alkalinity of a solution, which plays a crucial role in manufacturing and process industries, including pharmaceutical, chemical, food and beverage, and mineral water, in monitoring environment samples such as soil, rain, ocean, sea, and river, and in diagnoses of disease conditions [1–3]. The necessity for pH control is based on producing products with consistent and well-defined properties, enhancing production efficiency, safeguarding consumer health, and meeting regulatory requirements [4,5]. Any significant variance in system pH negatively affects critical process parameters during manufacturing and the quality of the final products, including their flavor, taste, consistency, safety, stability, and shelf-life [6,7].

Currently, there are two principal methods for measuring pH: colorimetric methods using indicator solutions or papers, and electrochemical methods using electrodes and a voltmeter (pH meter). Technological advancements in glass electrodes and pH meters have enabled electrochemical methods to become more reliable, accurate, and convenient in various applications [8]. However, various factors, including electrical and mechanical properties of the electrodes, ionic strength, temperature, and so on, determine the accuracy of pH measurement. Long-term pH measurement is also affected by electrode deterioration, the occurrence of liquid junction potential, and poor cleaning and calibration [9,10]. These factors, in turn, increase the operation cost of electrochemical methods.

Colorimetry, which is classified as traditional analytical technology, is subdivided into visual colorimetry (i.e., colorimetry that uses the naked eye to determine the color of a target solution) and photoelectric colorimetry (i.e., colorimetry that utilizes a spectrophotometer to measure the color) [11,12]. The former is less reliable than the latter, despite its benefits, such as simplicity, portability, cost-effectiveness, and small sample requirements.

Recent technological advancements in digital image acquisition enable colorimetry to be explored further than ever. Thus, fast, simple,

* Corresponding author at: Graduate School of Pharmaceutical Sciences, Tokushima University, 1-78-1 Shomachi, Tokushima 770-8505, Japan.
E-mail address: h.tanaka@tokushima-u.ac.jp (H. Tanaka).

https://doi.org/10.1016/j.talo.2023.100279
Received 3 October 2023; Received in revised form 13 November 2023; Accepted 5 December 2023
Available online 6 December 2023

cost-effective, and eco-friendly qualitative and quantitative analytical methods based on digital image-based colorimetry (DIC) have been developed [13,14]. DIC uses different color systems, such as RGB, HSV, CMYK, XYZ, L*a*b*, and Gray models, for qualitative description and quantitative determination of the substance of analytical interest. In these color systems, digital color analyzers transform the color information into numerical values that can be treated as analytical information. Color identification and quantification are done using various image analysis software [15].

RGB-based DIC works by converting pixel intensities of the sample images acquired by digital imaging devices, such as digital cameras, smartphones, webcams, and scanners, into analytical information through an image processing algorithm by splitting the image into red, green, and blue channels [16]. It establishes a correlation between channel intensity and sample color. A literature survey demonstrates that RGB-based DIC has been successfully applied to determine pH or analyte concentration in varied matrix samples such as solutions [17], cellular organisms [18], pharmaceutical formulations [19,20], urine samples [21], environmental samples [22,23], and foods and beverages [24–26]. Our group successfully integrated RGB-based DIC into flow-based titrimetry and determined the equivalence point based on the inner product of RGB unit vectors [27,28].

In the present paper, we report a simple, continuous, cost-effective, and versatile flow-based pH measurement method coupled with a digital-movie-based colorimetry using universal indicators (Yamada's and Van Urik's indicators). The indicator's color was expressed as the RGB values, hue, and luminance. Among these color specification values (CSV), hue showed the most distinct relationship to pH. Van Urik's indicator had a wider applicable pH range than Yamada's. The pH of a sample solution was estimated through a sigmoid-like calibration curve of hue vs. pH. The developed method was successfully applied to measure the pH of drug and vinegar samples.

Experimental

Materials

The reagents used in the present study were of analytical reagent grade and were purchased from Fujifilm Wako Pure Chemicals Co., Kanto Chemicals Co., Nacalai Tesque, or Kishida Chemical, Co., Japan. Deionized water (18.2 MΩ), daily prepared with Satoriums arium® 611DI ultrapure water system, was used throughout the experiment. The acid solution for Britton-Robinson buffer (BR buffer) was prepared by dissolving 4.61 g of 85 % phosphoric acid (H_3PO_4), 2.47 g of boronic acid (H_3BO_3), and 2.42 g of acetic acid (CH_3COOH) in the deionized water to make the final volume of 1 dm^3; the basic solution for the buffer was prepared by dissolving 8 g of sodium hydroxide (NaOH) in the deionized water, according to the literature [29]. Buffer solution (pH 2 – 12) was produced by merging both solutions in the flow system, as described later. Yamada's universal indicator was prepared by dissolving 5 mg of Thymol Blue, 12.5 mg of Methyl Red, 60 mg of Bromothymol Blue, and 100 mg of Phenolphthalein in 100 cm^3 of 95 % ethanol, being neutralized with 0.05 mol dm^{-3} NaOH, and then making the final volume of 200 cm^3 with the deionized water; Van Urik's universal indicator was prepared by dissolving 70 mg of Tropaeolin OO, 100 mg of Methyl Orange, 80 mg of Methyl Red, 400 mg of Bromothymol Blue, 500 mg of Naphtholphthalein, 400 mg of Cresolphthalein, 500 mg of Phenolphthalein, and 150 mg Alizarine Yellow R in 200 cm^3 ethyl alcohol [30]. For colorimetric measurements, 5 drops of Van Urik's indicator or 15 drops of Yamada's indicator (ca. 3.1 and 9.1 vol%, respectively, as final percentages) was added per 10 mL of the acid and base solutions for BR buffer.

Gentamycin 0.3 % ophthalmic solution purchased from Rohto Nitten, glucose injection, 5 % and Lactec® injection (principal agent: 0.3 % sodium L-lactate) from Otsuka Pharmaceutical Co., and sodium borate from Ken-ei Pharmaceutical Co. are Japanese Pharmacopoeia drugs. Apple and potato vinegar samples were purchased at a local supermarket in Tokushima City.

Flow system and methods

The schematic diagram of the flow system is presented in Fig. 1(A). Two peristaltic pumps (P_1 and P_2; Rainin Dynamax® RP-1, USA and Gilson Miniplus 3®, USA, respectively), each with 10 stainless-steel rollers, were used for delivering solutions. Pharmed® BPT AY242605 tubing (0.5 mm i.d., 3.2 mm o.d.) was used as pump tubing. Conduits for sample transport were PTFE tubing (0.5 mm i.d., 1.6 mm o.d.). A specially designed digital microscope-based detector (D_1; Shikoku Riken, SR700004–001, Japan) was used for digital video acquisition. The photograph of the inside of the detector is shown in Fig. 1(B). The detector mainly comprised a digital microscope (Sanwa Supply, 400-CAM058, Taiwan), a flow cell, an X-Z stage (As One, X14–102, Japan), and white LEDs located back and side to the cell. The cell is a 4-sided permeable rectangular quartz flow cell (3 mm i.d., 5.5 mm o.d., 30 mm length) manufactured by Optical Polishing OTG Co., Japan. A flow-through combination pH-reference electrode (Toa DKK Co., GST-5820C, Japan) and a pH meter (D_2; Toa DKK Co., HM-42X, Japan) were used for pH measurements.

The pH measurements were carried out in both variable and steady modes. In the variable mode, the flow rate of the base solution (F_B) for BR buffer containing either Yamada's universal indicator or Van Urik's universal indicator was varied in the range of 0 to 2.75 $cm^3\ min^{-1}$ with P_1, whose revolution was varied from 0 to 45 rpm in proportion to control voltage (V_c; 0 – 5 V) supplied from a laptop computer (Mouse, 20034N—CML-CPSC, Japan) via an A/D-D/A converter (CONTEC, AIO-160802GY-USB, Japan). While the flow rate (F_T) was kept constant at 2.93 $cm^3\ min^{-1}$ using P_2, the acidic solution for BR buffer containing the same concentration of the universal indicator was passively aspirated to the confluence point at a flow rate of $F_T - F_B$ and merged with the basic solution. The buffer solution, thus prepared, was introduced to the above-mentioned flow cell, where the digital video image of the colored solution was captured. The image data (IMG) was acquired in PC using Open Computer Vision (ver. 2.4.13) at a frequency of 10 Hz. The image's color was expressed as tristimulus values (RGB values) for each pixel in a preset range (6 × 6 pixels). The values were respectively averaged and used for further analysis. The solution was then introduced to the flow-through combination electrode. The output of the pH meter was converted to digital data (V_d) by the A/D-D/A converter and acquired in PC. The whole system was monitored by an in-house program written in Visual Basic .NET.

In the steady mode, the flow ratio of the acidic and basic solutions containing the same universal indicator was fixed at a specific value. The mixed solution's RGB values and pH were measured downstream sequentially. After obtaining steady analytical signals (i.e., RGB values and pH), the flow ratio was changed to the next value.

Results and discussion

Steady mode relationship between CSV and pH

The RBG color space assigns the primary color of red (700.0 mm), green (546.1 mm), and blue (435.8 mm). Any color is specified by the tristimulus values (*R, G, B*), each having a value from 0 to 255. Therefore, the color of the indicators can be expressed by these RGB values. In the present study, the image's RGB values were further converted to hue (0 – 360) and luminance (0 – 255), as shown in Table S1 in the Supplementary material.

Fig. 2A and 2B show the relationships between the color specification values CSV (*R, G, B*, hue, luminance) and pH for Yamada's and Van Urik's indicators, respectively, obtained in the steady mode. The color of both indicators was changed from red to violet via orange, yellow, green, and blue as the pH increased and vice versa as it decreased.

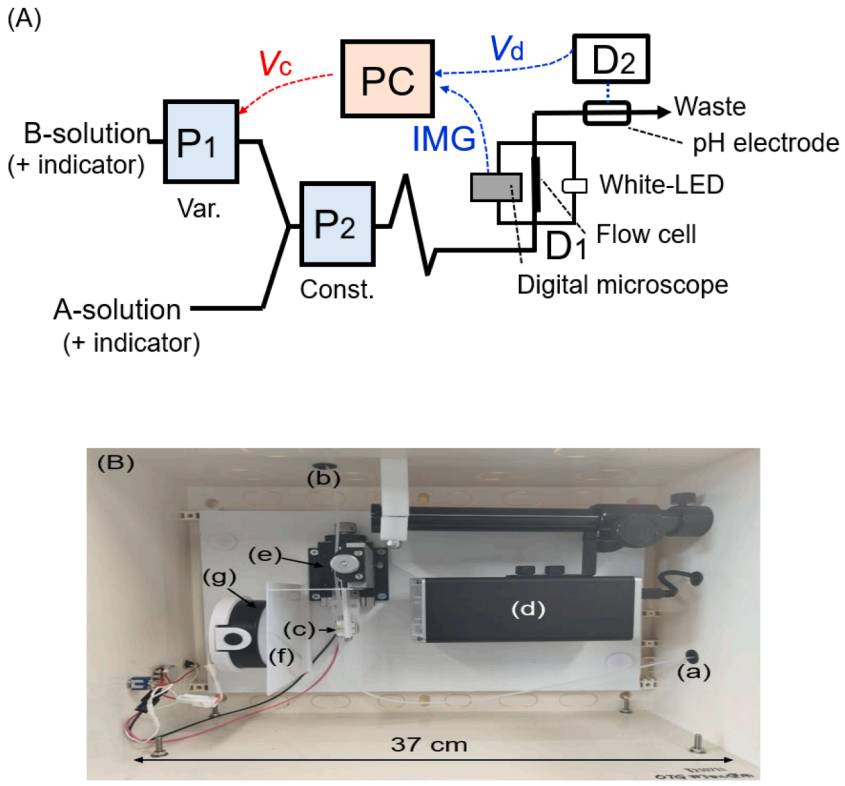

Fig. 1. (A) The schematic diagram of the experimental system. (B) Photograph of the inside of a specially designed digital microscope-based detector. (a) Inlet, (b) outlet, (c) flow cell, (d) digital microscope, (e) X-Z stage, (f) semi-transparent white plastic plate, (g) white LEDs.

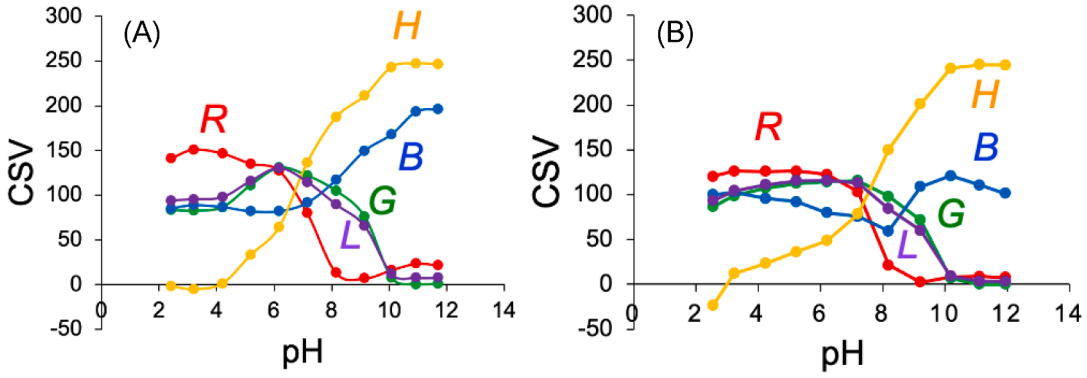

Fig. 2. Relationship between color specific values and pH at steady mode using Yamada's indicator (A) and Van Urik's indicator (B). H, hue; L, luminance. Hue from 330 to 360 are expressed as negative values (i.e., hue - 360) to maintain the continuity of the graph.

Among CSV, hue showed a strong positive correlation with pH for both indicators. Van Urik's showed a broader response range (pH 2.5 – 10) compared with Yamada's indicator (pH 4 – 10). The steady mode is expected to give more precise relationships between CSV and pH than the variable mode described below. However, obtaining stable values at each flow ratio took a long time (typically 2.2 min or more). It is not practical to further increase the number of measurement points. Therefore, we explored the variable mode to obtain a continuous relationship between CSV and pH.

Variable mode relationship between CSV and pH

In the variable mode, the flow ratio of A and B solutions, thus the pH of the merged solution, continuously changes via V_c (0 – 5 V). Therefore, continuous relationships between CSV and pH can be obtained without interruption. The V_c scan rate was examined in the 5 – 200 mV s^{-1} range. Although a higher scan rate is preferable to reduce the analytical time, the detectors cannot follow the rapid changes in color and pH. On the other hand, a slower scan rate (e.g., 5 mV s^{-1}) is expected to provide more accurate and precise results. However, it significantly increases analytical time (2000s to cover from 0 to 5 V in V_c and back), increasing reagent consumption. As a compromise, 10 mV s^{-1} was selected as the optimum scan rate. Under this condition, the time and the total consumption volume of the reagent solutions per one cycle of V_c scan were 1000s (= 5000 mV × 2 / (10 mV s^{-1}) and 48.8 cm^3 (= (1000/60 min) × 2.93 cm^3 min^{-1}), respectively. Fig. 3 shows the temporal profiles of V_c (A) and CSV (B) at the V_c scan rate of 10 mV s^{-1} for Van Urik's indicator. In our program, the hue value was expressed as a negative value (i.e., hue – 360) when it decreases, passes through 0, and takes a value between 330 and 360 to maintain the continuity of the graph. Fig 3(B) shows that the CSV values periodically and continuously changed following the V_c change (Fig. 3(A)). Among CSV, hue showed the most

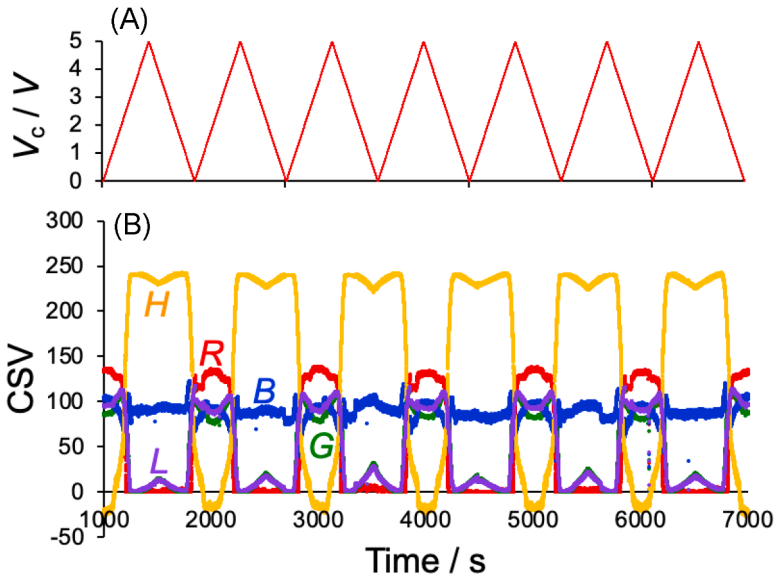

Fig. 3. Temporal profile of V_c (A) and CSV (B) for Van Urik's indicator. The scan rate of V_c was 10 mV s^{-1}. *H*, hue; *L*, luminance.

distinct relationship against pH, as in the steady mode. Similar results were obtained for Yamada's indicator (Fig. S1 in the Supplementary material).

In the present flow configuration, V_c determines the flow ratio of the acid and base solutions, hence the pH of the merged solution at the confluence point. However, there are three kinds of lag time, as shown in Fig. S2 in the Supplementary material: lag time (t_{lag1}) from the merging to the color sensing, that (t_{lag2}) from the merging to the pH sensing, and that (t_{lag2-1}) from the color sensing to the pH sensing. The t_{lag1} virtually corresponds to the physical transit time of the merged solution to reach the first detector D_1 (digital microscope-based detector) because the response of the image detector is fast. The t_{lag1} can be regarded as constant because of the constant total flow rate (F_T). The second lag time (t_{lag2}) combines primarily the physical transit time of the merged solution to reach the second detector D_2 (pH meter) and minutely the response time of the glass electrode. Therefore, correcting the phase differences between V_c, IMG, and V_d is crucial to obtain their true relationships.

Fig. 4 shows hue (red) and pH (blue) as a function of V_c for Van Urik's indicator. Both plots showed closed-loop profiles due to the lag time (t_{lag1} and t_{lag2}, respectively). That is, when hue corresponding to a given V_c is obtained downstream, V_c being applied upstream has already moved to a higher or lower value by $t_{lag1} \times dV_c/dt$ in the upward or downward V_c scan, respectively, where dV_c/dt means the V_c scan rate. A similar discussion using t_{lag2} is valid for the relationship between pH and V_c. Therefore, the horizontal V_c distance (ΔV_c) of the loop can be expressed as follows,

$$\Delta V_c = 2\, t_{lag} \times \frac{dV_c}{dt}, \quad (1)$$

where t_{lag} is t_{lag1} or t_{lag2}. Eq. (2) is derived from Eq. (1).

$$t_{lag} = \Delta V_c \Big/ \left(2\,\frac{dV_c}{dt}\right) \quad (2)$$

The t_{lag1} and t_{lag2} were calculated from ΔV_c at half height of the hue and pH loops (110.00 and 7.00, respectively) shown by the horizontal lines (a) and (b) in Fig. 4. The estimated t_{lag1} and t_{lag2} were 9.40 s and

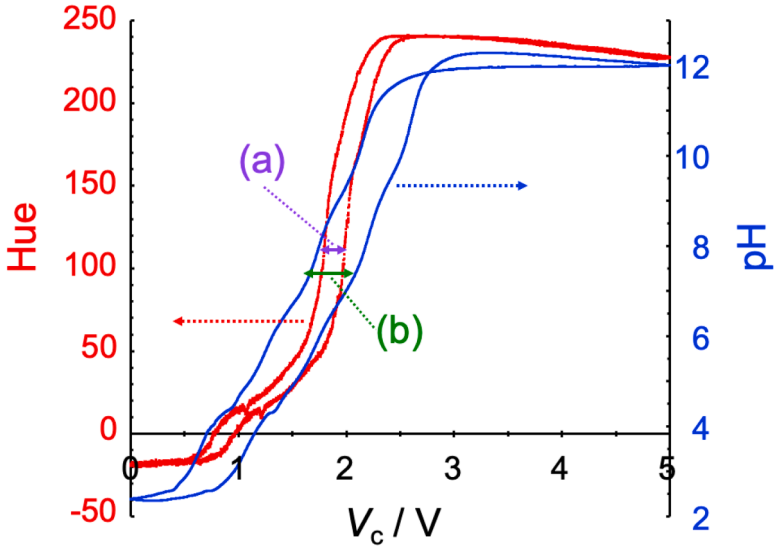

Fig. 4. Hue and pH as a function of V_c. The data shown in Fig. 3 were used. V_c difference (ΔV_c) at the half heights of the loops was expressed by the horizontal purple (a) and green (b) arrows for hue and pH, respectively.

20.80 s, respectively. Subtracting t_{lag1} from t_{lag2} gives the lag time between the color and pH sensing, t_{lag2-1}, which was obtained to be 11.40 s.

Fig. 5(A) shows the relationship between hue and pH before (red) and after (orange) the correction for t_{lag2-1} for Van Urk's indicator. The loop shape almost disappeared through the correction, and the true relationship between hue and pH could be established. The relationship is of a sigmoid-like profile, which can be used as a calibration curve for estimating pH from hue. Fig. 5(B) shows the relationships between all CSV (i.e., *R, G, B*, hue, luminance) and pH after t_{lag2-1} correction.

The results for Yamada's indicator correspond to Figs. 4, 5(A), and 5 (B) are respectively shown in Fig. S3(A), (B), and (C) in the Supplementary material. Whereas Van Urik's indicator consists of eight acid-base indicators with respective color transition ranges, Yamada's indicator consists of only four indicators, resulting in a narrower applicable pH range (4.5 – 10.0) and more pronounced shoulders in the calibration curve (see orange curve in Fig. S3(B)).

Application to real samples

The newly developed digital-movie-based colorimetry for continuous pH monitoring was applied to determine the pH of real samples. Sample products were selected so that the pH of themselves or their aqueous solutions could cover acidic, neutral, and basic pH ranges. All tested drug products comply with pharmacopeia specification and product label claim for pH. The hue values of sample solutions containing 3.1 vol% of the Van Urik's universal indicator were measured by each delivering from both channels at a total flow rate of 2.93 $cm^3\ min^{-1}$ shown in Fig. 1(A). The pH of the sample solutions (pH_{hue}) was estimated using the calibration curve (hue vs. pH) shown in Fig. 5. Besides, their pH values ($pH_{electrode}$) were measured with the flow-through combination glass electrode, as references. The results are listed in Table 1. The pH_{hue} agreed well with $pH_{electrode}$ ($P > 0.05$ by *t*-test), except Gentamycin 0.3 % ophthalmic solution ($P = 0.00014$) and apple vinegar ($P = 0.020$). A colloidal suspension was formed during the Gentamycin measurement. Whereas the potato vinegar had a faint yellow color, the apple vinegar itself had a deeper brownish color. The proposed hue-based method is, therefore, suitable for samples that produce no precipitation or for virtually colorless samples.

In practice, estimating pH_{hue} from hue using the nonlinear calibration curve shown in Fig. 5 is cumbersome. From a practical viewpoint, a linear calibration curve is preferable. Therefore, we also investigated a method for expressing data as a linear relationship. The calibration curve is of a sigmoid-like profile. Therefore, a logistic function, $y = K/[1 + exp\{-a(x - b)\}]$, was applied to the relationship between hue and pH, as follows:

Table 1
Real samples' pH determined by the present and reference methods.

Sample	Proposed method		Reference method
	Hue[a]	pH_{hue}[b]	$pH_{electrode}$
Sodium borate	225.09 ± 0.84	9.62 ± 0.13	9.61 ± 0.02[c]
Gentamycin 0.3 % ophthalmic solution[d]	203.17 ± 2.41	9.09 ± 0.20	6.54 ± 0.01[c]
Lactec® injection[e]	51.01 ± 2.83	6.61 ± 0.07	6.49 ± 0.01[a]
Deionized water	30.47 ± 1.72	5.46 ± 0.05	5.62 ± 0.05[a]
Glucose injection 5 %[f]	24.54 ± 1.85	5.07 ± 0.05	5.13 ± 0.15[a]
Apple vinegar	7.74 ± 1.11	3.63 ± 0.06	3.34 ± 0.01[a]
Potato vinegar	−12.66 ± 2.69	2.91 ± 0.04	2.85 ± 0.11[a]

pH_{hue}: pH estimated from hue using the calibration curve shown in Fig. 5. $pH_{electrode}$: pH measured with flow-through grass electrode and pH meter. $n =$ [a] 2, [b] 2, [c] 3. Labeled pH value: [d] 5.5 – 7.5, [e] 6.0 – 7.5, [f] 3.5 – 6.5.

$$\text{Hue} = \frac{360}{1 + \exp\{-a(\text{pH} - b)\}}, \tag{3}$$

where *b* is the pH that gives the inflection point. From Eq. (3), the following equation was derived.

$$\ln\frac{\text{Hue}}{360 - \text{Hue}} = a\text{pH} - ab \tag{4}$$

Therefore, a linear calibration curve with slope *a* and intercept *ab* can be obtained by plotting ln{Hue/(360 – Hue)} against pH. Fig. 6 shows the plot based on Eq. (4). The shoulders in the plot reflected the color transition of respective acid-base indicators. Therefore, linear calibration curves were respectively obtained for the pH ranges of 4.6 – 6.2, 6.2 – 7.3, 7.3 – 8.2, and 8.2 – 9.8, which corresponded to the color transition ranges of Methyl Red (4.4 – 6.2), Bromothymol Blue (6.0 – 7.6), Naphtolphthalein (7.3 – 8.7), and Cresolphthalein (8.2 – 9.8)· Phenolphthalein (8.0 – 10.0) [31]. The obtained calibration curves are shown in Fig. 6, the linearities of which are fairly well ($r^2 = 0.9368$ – 0.9785). Reasonable pH values with an absolute error of less than ±0.05 from pH_{hue} were obtained: 9.61 for sodium borate, 6.56 for Lactec® injection, 5.51 for deionized water, and 5.08 for Glucose injection 5 %. Therefore, under the compromise of the error of ±0.05, linear calibration curves (Fig. 6) based on Eq. (4) are considered to be a convenient alternative to the sigmoid-like calibration curve shown in Fig. 5.

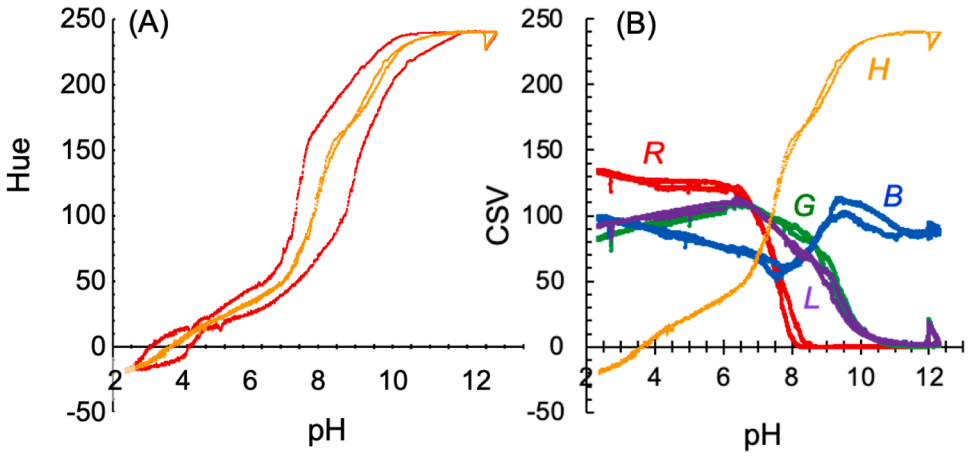

Fig. 5. (A) Relationship between hue and pH before and after t_{lag2-1} correction. (B) Compiled results for all CSV vs. pH after t_{lag2-1} correction. Indicator: Van Urik's indicator. *H*, hue; *L*, luminance.

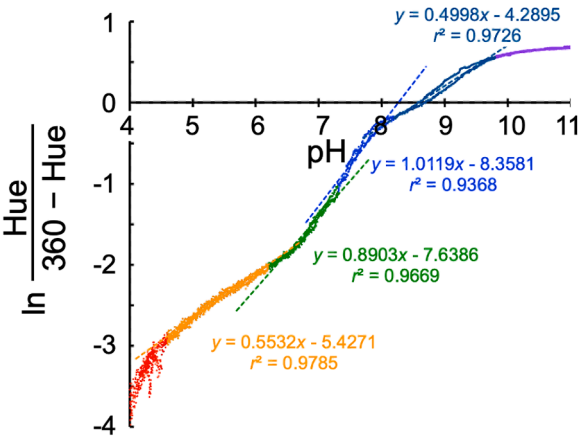

Fig. 6. Linear calibration curve fitting with a logistic function for pH ranges of 4.6 – 6.2 (orange), 6.2 – 7.3 (green), 7.3 – 8.2 (blue), and 8.2 – 9.8 (indigo).

However, as for the potato vinegar, Eq. (4) was not applicable because of its negative antilogarithm value. It should be noted that the same results were obtained even if one additional parameter c was introduced to Eq. (3) (i.e., Hue = 360/[1 + c exp{−a(pH − b)}]).

Conclusion

A digital-movie-based colorimetry for continuous pH monitoring has been developed to determine pH with a high accuracy, precision, and reliability without the need for indicator change. The relationship between pH and hue of universal indicators (Van Urk's and Yamada's indicators) was established. Besides, the analytical system is continuous, easy to operate, economical, fast, eco-friendly, and stable. As a result, it can be used as an alternative method for existing pH determination methods except for precipitate-forming or colored samples. The system could be applied for pH monitoring of environmental samples such as oceans, lakes, and river waters and industrial samples such as raw materials and intermediate and final products.

Declaration of Competing Interest

The authors declare that they have no known competing financial interests or personal relationships that could have appeared to influence the work reported in this paper.

Data availability

Data will be made available on request.

Acknowledgments

The authors would like to express their gratitude to Dr. Akira Ohbuchi, Professor Emeritus of Tokushima University, for his advice on logistic functions. The present study is partly supported by a Grant-in-Aid for Scientific Research (C) (21K05127) from the Japan Society for the Promotion of Sciences (JSPS).

Supplementary materials

Supplementary material associated with this article can be found, in the online version, at doi:10.1016/j.talo.2023.100279.

References

[1] R.G. Bates, A.K. Vijh, Determination of pH: theory and practice, J. Electrochem. Soc. 120 (1973) 263C, https://doi.org/10.1149/1.2403829.
[2] S. Rahman, Handbook of Food Preservation, 3rd ed., CRC Press, Boca Raton, 2020 https://doi.org/10.1201/9781420017373.
[3] K. Farley, E. Licari, A structured approach to acid-base interpretation, Med. J. Aust. 211 (2019) 308, https://doi.org/10.5694/mja2.50344.
[4] J. Naceradska, L. Pivokonska, M. Pivokonsky, On the importance of pH value in coagulation, J. Water Supply Res. Technol. Aqua 68 (2019) 222–230, https://doi.org/10.2166/aqua.2019.155.
[5] J.B. Russell, The importance of pH in the regulation of ruminal acetate to propionate ratio and methane production *in vitro*, J. Dairy Sci. 81 (1998) 3222–3230, https://doi.org/10.3168/jds.S0022-0302(98)75886-2.
[6] F. Simoes, P. Vale, T. Stephenson, A. Soares, The role of pH on the biological struvite production in digested sludge dewatering liquors, Sci. Rep. 8 (2018) 7225, https://doi.org/10.1038/s41598-018-25431-7.
[7] C. Tudisco, B.W. Jett, K. Byrne, J. Oblitas, S.F. Leitman, D.F. Stroncek, The value of pH as a quality control indicator for apheresis platelets, Transfusion 45 (2005) 773–778, https://doi.org/10.1111/j.1537-2995.2005.04344.x.
[8] R.P. Buck, S. Rondinini, A.K. Covington, F.G.K. Baucke, C.M.A. Brett, M.F. Camoes, M.J.T. Milton, T. Mussini, R. Naumann, K.W. Pratt, P. Spitzer, G.S. Wilson, Measurement of pH, definition, standards, and procedures, Pure Appl. Chem. 74 (2002) 2169–2200, https://doi.org/10.1351/pac200274112169.
[9] C. Emde, R. Hopert, E.O. Riecken, Basic principles of pH registration, Neth. J. Med. 34 (S3–9) (1989). PMID: 2725802.
[10] B. Anes, R.J.N. Bettencourt da Silva, C. Oliveira, M.F. Camões, Seawater pH measurements with a combination glass electrode and high ionic strength– an uncertainty evaluation approach, Talanta 193 (2019) 118–122, https://doi.org/10.1016/j.talanta.2018.09.075.
[11] F.M. Clydesdale, E.M. Ahmed, Colorimetry – methodology and applications, Crit. Rev. Food Sci. Nutr. 10 (1978) 243–301, https://doi.org/10.1080/10408397809527252.
[12] S. Wu, D. Li, J. Wang, Y. Zhao, S. Dong, X. Wang, Gold nanoparticles dissolution based colorimetric method for highly sensitive detection of organophosphate pesticides, Sens. Actuators B Chem. 238 (2017) 427–433, https://doi.org/10.1016/j.snb.2016.07.067.
[13] E. da Nobrega Gaiao, V.L. Martins, W.da S. Lyra, L.F. de Almeida, E.C. da Silva, M. C.U. Araújo, Digital image-based titrations, Anal. Chim. Acta 570 (2006) 283–290, https://doi.org/10.1016/j.aca.2006.04.048.
[14] L. Byrne, J. Barker, G. Pennarun-Thomas, D. Diamond, S. Edwards, Digital imaging as a detector for generic analytical measurements, Trends Anal. Chem. 19 (2000) 517–522, https://doi.org/10.1016/S0165-9936(00)00019-4.
[15] Y. Fan, J. Li, Y. Guo, L. Xie, G. Zhang, Digital image colorimetry on smartphone for chemical analysis: a review, Measurement 171 (2021), 108829, https://doi.org/10.1016/j.measurement.2020.108829.
[16] J. Caleb, U. Alshana, N. Ertaş, Smartphone digital image colorimetry combined with solidification of floating organic drop-dispersive liquid-liquid microextraction for the determination of iodate in table salt, Food Chem. 336 (2021), 127708, https://doi.org/10.1016/j.foodchem.2020.127708.
[17] Z. Rasouli, H. Abdollahi, M. Maeder, Generalized indicator-based determination of solution pH, Anal. Chim. Acta 1109 (2020) 90–97, https://doi.org/10.1016/j.aca.2020.03.004.
[18] P. Srivastava, I. Tavernaro, C. Genger, P. Welker, O. Hübner, U. Resch-Genger, Multicolor polystyrene nanosensors for the monitoring of acidic, neutral, and basic pH values and cellular uptake studies, Anal. Chem. 94 (2022) 9656–9664, https://doi.org/10.1021/acs.analchem.2c00944.
[19] I. Berasarte, A. Bordagaray, R. Garcia-Arrona, M. Ostra, M. Vidal, pH measurement and phosphate determination in pharmaceutical eye drops for eye diseases by digital image analysis, Microchem. J. 162 (2021), 105854, https://doi.org/10.1016/j.microc.2020.105854.
[20] R. Urapen, P. Masawat, Novel method for the determination of tetracycline antibiotics in bovine milk based on digital-image-based colorimetry, Int. Dairy J. 44 (2015) 1–5, https://doi.org/10.1016/j.idairyj.2014.12.002.
[21] A.W. Martinez, S.T. Phillips, E. Carrilho, S.W. Thomas, H. Sindi, G.M. Whitesides, Simple telemedicine for developing regions: camera phones and paper-based microfluidic devices for real-time, off-site diagnosis, Anal. Chem. 80 (2008) 3699–3707, https://doi.org/10.1021/ac800112r.
[22] S.I.E. Andrade, M.B. Lima, I.S. Barreto, W.S. Lyra, L.F. Almeida, M.C.U. Araújo, E. C. Silva, A digital image-based flow-batch analyzer for determining Al(III) and Cr (VI) in water, Microchem. J. 109 (2013) 106–111, https://doi.org/10.1016/j.microc.2012.03.029.
[23] S. Sumriddetchkajorn, K. Chaitavon, Y. Intaravanne, Mobile-platform based colorimeter for monitoring chlorine concentration in water, Sens. Actuators B Chem. 191 (2014) 561–566, https://doi.org/10.1016/j.snb.2013.10.024.
[24] A.R. Tôrres, W. Da Silva Lyra, S.I.E. De Andrade, R.A.N. Andrade, E.C. Da Silva, M. C.U. Araújo, E.A. Da Nóbrega Gaião, Digital image-based method for determining of total acidity in red wines using acid–base titration without Indicator, Talanta 84 (2011) 601–606, https://doi.org/10.1016/j.talanta.2011.02.002.
[25] V. Kumar, R.S. Aulakh, J.P.S. Gill, A. Sharma, Exploring smart phone based colorimetric technology for on-site quantitative determination of adulterant (neutralizer) in milk, J. Food Sci. Technol. 59 (2022) 3693–3699, https://doi.org/10.1007/s13197-022-05392-6.
[26] L. Pires Dos Santos Benedetti, V. Bezerra Dos Santos, T.A. Silva, E. Benedetti-Filho, V.L. Martins, O. Fatibello-Filho, A digital image analysis method for quantification of sulfite in beverages, Anal. Methods 7 (2015) 7568–7573, https://doi.org/10.1039/C5AY01372K.
[27] N. Kakiuchi, J. Ochiai, M. Takeuchi, H. Tanaka, Inner product of RGB unit vectors for simple and versatile detection of color transition, Anal. Sci. 37 (2021) 3–5, https://doi.org/10.2116/analsci.20C015.

[28] N. Kakiuchi, J. Ochiai, M. Takeuchi, H. Tanaka, Inner product of RGB unit vectors for detecting color transition: application to feedback-based flow ratiometric titration, Anal. Sci. 38 (2022) 623–626, https://doi.org/10.1007/s44211-022-00075-w.

[29] H.T.S. Britton, R.A. Robinson, Universal buffer solutions and the dissociation constant of veronal, J. Chem. Soc. 0 (1931) 1456–1462, https://doi.org/10.1039/JR9310001456.

[30] L.S. Foster, I.J. Gruntfest, Demonstration experiments using universal indicators, J. Chem. Educ. 14 (1937) 274, https://doi.org/10.1021/ed014p274.

[31] R.W. Sabnis, Handbook of Acid-Base Indicators, CRC Press, Baca Raton, 2019.